Available online at www.sciencedirect.com

ScienceDirect

IFAC PapersOnLine 59-20 (2025) 1930–1935

Continuous Constrained Predictive Control for Quadrotor Trajectory Tracking with Obstacle Avoidance

Somayeh Jamshidi*, Maria Khodaverdian**, Mehdi Mirzaei*, Paolo Castaldi***

* *Faculty of Mechanical Engineering, Sahand University of Technology, Sahand new town, P.O. Box 51335-1996, Tabriz, Iran (emails: so_jamshidi98@sut.ac.ir, Mirzaei@sut.ac.ir)*

** *National Polytechnic University of Armenia, and the Center for Scientific Innovation and Education, Yerevan, Armenia (email: mariakhodaverdian@gmail.com)*

*** *Department of Electrical, Electronic and Information Engineering University of Bologna, Forlí (FC), Italy (email: paolo.castaldi@unibo.it)*

Abstract: In this study, a continuous constrained dual-loop predictive control method is proposed for trajectory tracking of quadrotor unmanned aerial vehicle, considering both physical and environmental restrictions. Using the predictive approach, the operational constraints of the quadrator are formulated and incorporated into an optimal control framework. The constrained control law is then derived by solving an equivalent optimization problem. The stability of the constrained closed-loop system is analyzed using Lyapunov's second method, and the system's response bounds are determined in terms of prediction time. The effectiveness of the proposed approach is validated through computer simulations. A comparative analysis with existing literature demonstrates that the proposed method efficiently combines trajectory tracking and obstacle avoidance while remaining computationally feasible.

Keywords: Constrained optimization, Dual-loop predictive control, Obstacle avoidance, Quadrotor trajectory tracking.

1. INTRODUCTION

The field of quadrotor Unmanned Aerial Vehicle (UAV) has seen significant advancements in recent years, driven by their growing applications in industrial and technological domains. Among the various research challenges in UAV control, trajectory tracking remains a fundamental problem, particularly in control and robotics (Lee and Kim, 2017). Achieving precise trajectory tracking requires advanced control strategies capable of handling system dynamics, external disturbances, and environmental uncertainties while maintaining computational efficiency for real-time execution (Wang and Boyle, 2024).

A key challenge in UAV trajectory tracking is satisfying constraints like input limits and obstacle avoidance, as neglecting them can cause instability or mission failure (Zhao et al., 2021). Researchers have explored various approaches to mitigate obstacle avoidance issue, including constrained path planning algorithms and constrained trajectory tracking control methods.

In the context of path planning, several studies have focused on generating collision-free trajectories. For instance, Yu et al. (2019) proposed a method that integrates Markov decision processes with differential flatness to compute safe trajectories. Similarly, Wen et al. (2015) introduced a receding horizon-based approach combined with the rapidly-exploring random tree (RRT) algorithm to navigate dense obstacle environments. Additionally, Wang et al. (2022) developed a hybrid path planning algorithm that integrates the A^* search method with potential field techniques. Finally, Li et al. (2025) proposes an MPC-based online planner that adjusts the reproduced trajectory to avoid collisions in the presence of obstacles. Although these methods demonstrate effective path planning capabilities, they often suffer from high computational complexity, making them challenging for real-time UAV applications with limited onboard processing power.

Beyond path planning, extensive research has been conducted on integrating constraint-handling techniques directly into UAV control strategies. Model Predictive Control (MPC) has been widely used for optimizing UAV trajectory tracking under constraints (Khodaverdian et al., 2025; Lin et al., 2024). Wang et al. (2024) proposed a dual MPC approach that leverages control Lyapunov and control barrier functions to maintain formation and ensure collision avoidance in multi-quadrotor systems. While classical MPC suits linear systems, applying it to nonlinear UAVs is computationally demanding and often overlooks uncertainties and disturbances, affecting real-world performance (Wang et al., 2022).

To address these limitations, this paper proposes a novel continuous predictive control strategy for UAV trajectory

Peer review under responsibility of International Federation of Automatic Control.
10.1016/j.ifacol.2025.11.440

tracking under operational constraints. Unlike existing approaches, the proposed method efficiently integrates trajectory tracking and obstacle avoidance while maintaining computational feasibility. By leveraging predictive modeling and optimization techniques, our approach ensures robust performance under system uncertainties with minimal computational overhead. The key contributions of this work are as follows:

- A predictive modeling framework based on Taylor series expansion is developed to estimate the future error dynamics of UAVs, allowing for the derivation of a constrained control law with low computational complexity.
- Stability is analyzed via Lyapunov's method, yielding response bounds and tuning insights.
- Trajectory tracking is validated via simulations, with improved performance over Sliding Mode Predictive Control (SMPC) (Kang et al., 2021) in multiple aspects.

The paper is organized as follows: in Section 2, the system modeling is presented. The control strategy formulation is discussed in Section 3, followed by the stability analysis in Section 4. Section 5 covers the simulation results. Finally, Section 6 presents the conclusion.

2. SYSTEM MODELING

The mathematical framework for quadrotor UAV dynamics is presented in this section, including both translational and rotational equations of motion. The governing equations presented here are based on previous research (Cabecinhas et al., 2014).The rotation matrix $\boldsymbol{R}_{\mathbb{B}}^{\mathbb{E}} \in SO(3)$ is used to describe the orientation of the UAV from the body frame to the earth frame, denoted as $\boldsymbol{R}_{\mathbb{B}}^{\mathbb{E}} : \mathbb{B} \longrightarrow \mathbb{E}$. This rotation matrix is orthonormal, and its expression is given by

$$\boldsymbol{R}_{\mathbb{B}}^{\mathbb{E}} = \begin{bmatrix} \mathrm{c}_\psi \mathrm{c}_\theta & \mathrm{s}_\theta \mathrm{s}_\phi \mathrm{c}_\psi - \mathrm{s}_\psi \mathrm{c}_\phi & \mathrm{c}_\phi \mathrm{c}_\psi \mathrm{s}_\theta + \mathrm{s}_\phi \mathrm{s}_\psi \\ \mathrm{c}_\theta \mathrm{s}_\psi & \mathrm{s}_\phi \mathrm{s}_\psi \mathrm{s}_\theta + \mathrm{c}_\phi \mathrm{c}_\psi & \mathrm{c}_\phi \mathrm{s}_\psi \mathrm{s}_\theta - \mathrm{s}_\phi \mathrm{c}_\psi \\ -\mathrm{s}_\theta & \mathrm{s}_\phi \mathrm{c}_\theta & \mathrm{c}_\phi \mathrm{c}_\theta \end{bmatrix}, \tag{1}$$

where $\mathrm{s}\wp = \sin(\wp)$ and $\mathrm{c}\wp = \cos(\wp)$ for $\wp = \phi, \theta, \psi$. The UAV's dynamics equations are expressed as

$$\dot{\boldsymbol{v}} = \frac{1}{m}(\boldsymbol{R}_{\mathbb{B}}^{\mathbb{E}} \boldsymbol{e}_3 f_{\mathrm{T}} - \mathbf{G}), \tag{2a}$$

$$\dot{\boldsymbol{\Omega}} = \boldsymbol{J}^{-1}\left(-\boldsymbol{\Omega}^{\times} \boldsymbol{J} \boldsymbol{\Omega} + \boldsymbol{\tau} + \boldsymbol{\tau}_{\mathrm{d}}\right), \tag{2b}$$

where, $\boldsymbol{v} \in \mathbb{R}^3$ is the linear velocity vector, $\boldsymbol{e}_3 = [0, 0, 1]^\top$ represents the unit vector along the z-axis, m denotes the total mass, $\boldsymbol{G} = [0 \quad 0 \quad mg]^\top$ corresponds to the gravitational force, where g is the acceleration due to gravity and $f_T \in \mathbb{R}$ refers to the thrust produced by the rotation of the rotors. The positive definite matrix $\boldsymbol{J} \in \mathbb{R}^{3\times3}$ represents the system's inertia, $\boldsymbol{\Omega}=[p \quad q \quad r]^\top \in \mathbb{R}^3$ is the angular velocity vector, $\boldsymbol{\tau} \in \mathbb{R}^3$ and $\boldsymbol{\tau}_d \in \mathbb{R}^3$ denote the control and disturbance torques. Additionally, the kinematics are described by

$$\dot{\boldsymbol{p}} = \boldsymbol{v}, \tag{3a}$$

$$\dot{\boldsymbol{\xi}} = \boldsymbol{T}_{(\phi,\theta)} \boldsymbol{\Omega}, \tag{3b}$$

where $\boldsymbol{p} \in \mathbb{R}^3$ is the position vector, $\boldsymbol{\xi} \in \mathbb{R}^3$ is Euler attitude and $\boldsymbol{T}_{(\phi,\theta)}$ is defined as

$$\boldsymbol{T}_{(\phi,\theta)} = \begin{bmatrix} 1 & \mathrm{s}_\phi \mathrm{t}_\theta & \mathrm{c}_\phi \mathrm{t}_\theta \\ 0 & \mathrm{c}_\phi & -\mathrm{s}_\phi \\ 0 & \frac{\mathrm{s}_\phi}{\mathrm{c}_\theta} & \frac{\mathrm{c}_\phi}{\mathrm{c}_\theta} \end{bmatrix}, \tag{4}$$

where $\mathrm{t}_\theta = \tan(\theta)$.

To facilitate further derivations, the second derivative of $\ddot{\boldsymbol{\xi}}$ can be obtained using the nominal dynamics given in (2b) as

$$\ddot{\boldsymbol{\xi}} = \dot{\boldsymbol{T}}_{(\phi,\theta)} \boldsymbol{\Omega} + \boldsymbol{T}_{(\phi,\theta)} \boldsymbol{f} + \boldsymbol{T}_{(\phi,\theta)} \boldsymbol{J}^{-1}(\boldsymbol{\tau} + \boldsymbol{\tau}_{\mathrm{d}}), \tag{5}$$

where $\boldsymbol{f} = \boldsymbol{J}^{-1}(-\Omega \times \boldsymbol{J}\Omega)$.

3. CONTINUOUS PREDICTIVE CONTROL STRATEGY FORMULATION

Given the quadrotor's underactuated nature, a dual-loop strategy is employed: the outer loop controls position by generating thrust and Euler angle commands, while the inner loop manages attitude and ensures precise trajectory tracking via torque control.
An optimization-based control law is designed to handle disturbances and physical constraints. By predicting system responses and solving a quadratic optimization problem, an optimal constrained controller is formulated. Spatial constraints and input constraints are integrated through a prediction-based transformation, ensuring practical and efficient control. Figure 1 illustrates the proposed control framework.

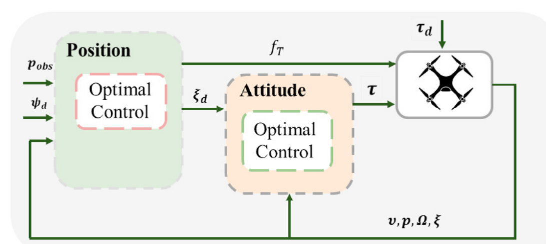

Fig. 1. The overview of the proposed algorithm.

3.1 Position Loop

This section designs an outer-loop controller that facilitates precise trajectory tracking by supplying roll and pitch commands to the inner loop. To continue with further derivations, we consider the nominal dynamics (2a), with the designed thrust f_{T}. The vector $\boldsymbol{u}_{\mathrm{p}} \in \mathbb{R}^3$, representing the virtual control input, is defined as

$$\boldsymbol{u}_p = \frac{1}{m}\left(\boldsymbol{R}_{\mathbb{B}}^{\mathbb{E}} \boldsymbol{e}_3 f_T - \boldsymbol{G}\right) = [u_x, u_y, u_z]^\top, \tag{6}$$

where the individual control inputs u_x, u_y, u_z, respectively associated with the translational motion along the x, y, z-axes, are described as

$$\begin{aligned} u_x &= \frac{1}{m}\left(c_\psi s_\theta c_\phi + s_\psi s_\phi\right) f_T, \\ u_y &= \frac{1}{m}\left(s_\psi s_\theta c_\phi - c_\psi s_\phi\right) f_T, \\ u_z &= \frac{1}{m}\left(c_\theta c_\phi\right) f_T - g. \end{aligned} \tag{7}$$

To derive a nonlinear position control law in closed form, a one-step-ahead predictive approach is utilized. This method predicts the future position $\boldsymbol{p}(t+h)$ using Taylor series expansion and determines the current control input $\boldsymbol{u}_p$ by minimizing the predicted tracking errors (Jamshidi et al., 2025).

By considering the UAV position as the system's output, a performance index that penalizes the next tracking error is defined as

$$I_1 = \frac{1}{2}[\boldsymbol{p}(t+h) - \boldsymbol{p}_d(t+h)]^\top [\boldsymbol{p}(t+h) - \boldsymbol{p}_d(t+h)]. \quad (8)$$

where, $\boldsymbol{p}_d(t+h) \in \mathbb{R}^3$ represents the desired position, and $h > 0$ is allocated for the prediction time.The future behavior of the output and the desired one should be approximated using a Taylor series. The order of expansion is limited by the output degree relative to the control input (Jamshidi et al., 2023). Since $\ddot{\boldsymbol{p}} = \boldsymbol{u}_p$, the control torque appears in the second derivative of the position and thus, the relative degree is $k = 2$. Therefore, the Taylor series expansion of the position and the desired one is given by

$$\begin{aligned} \boldsymbol{p}(t+h) =& \boldsymbol{p}(t) + h\dot{\boldsymbol{p}}(t) + \frac{h^2}{2!}\ddot{\boldsymbol{p}}(t), \\ \boldsymbol{p}_d(t+h) =& \boldsymbol{p}_d(t) + h\dot{\boldsymbol{p}}_d(t) + \frac{h^2}{2!}\ddot{\boldsymbol{p}}_d(t). \end{aligned} \quad (9)$$

In position control design, it is essential to account for position constraints, which include spatial limitations such as no-fly zones. The following condition ensures collision avoidance:

$$\|\boldsymbol{p} - \boldsymbol{p}_{obs}\|^2 \geq D^2, \quad (10)$$

where $\boldsymbol{p}_{obs} \in \mathbb{R}^3$ denotes the position coordinates of all fixed obstacles in the environment, and $D \in \mathbb{R}$ is the minimum distance. Following one-step-ahead prediction approach, the control input is designed to maintain the obstacle distance above the minimum allowable threshold at the next time step, meaning that

$$\|\boldsymbol{p}(t+h) - \boldsymbol{p}_{obs}\|^2 \geq D^2. \quad (11)$$

By considering Eq. (9) and $\boldsymbol{\eta} = \boldsymbol{p} - \boldsymbol{p}_{obs}$, the left-hand side of (11) is rewritten as

$$\eta^2 = \|\boldsymbol{p} + h\dot{\boldsymbol{p}} + \frac{h^2}{2!}\ddot{\boldsymbol{p}} - \boldsymbol{p}_{obs}\|^2. \quad (12)$$

After simplifying Eq. (12), it takes the following form

$$\eta^2 = \|\boldsymbol{p} + h\dot{\boldsymbol{p}} - \boldsymbol{p}_{obs}\|^2 + h^2(\boldsymbol{p} + h\dot{\boldsymbol{p}} - \boldsymbol{p}_{obs})^\top \mathbf{u}_p + \frac{h^4}{4}\mathbf{u}_p^\top \mathbf{u}_p. \quad (13)$$

The constraints must also be convex and linear with respect to $\mathbf{u}_p$. Given that Eq. (13) is nonlinear in $\mathbf{u}_p$, it is linearized around $\mathbf{u}_p = 0$ (Vargas et al., 2022). Note that, in highly nonlinear or concave environments, nonlinear constraints may lead to local minima and complicate the optimization process. In this work, obstacle constraints are linearized and treated as soft constraints to enable real-time implementation. Let $\bar{\boldsymbol{\eta}}$ represent the linearized approximation, which is defined as

$$\begin{aligned} \bar{\eta}^2 &= \eta^2(0) + \frac{\partial \eta^2(0)}{\partial \mathbf{u}_p}(\mathbf{u}_p - 0) \\ &= \|\boldsymbol{p} + h\dot{\boldsymbol{p}} - \boldsymbol{p}_{obs}\|^2 + h^2(\boldsymbol{p} + h\dot{\boldsymbol{p}} - \boldsymbol{p}_{obs})^\top \mathbf{u}_p. \end{aligned} \quad (14)$$

By considering (14), the constraint arising from the non-collision condition can be expressed as follows:

$$\mathbf{M}^\top \mathbf{u}_p \geq (D^2 - N), \quad (15)$$

where $\mathbf{M} = h^2(\boldsymbol{p} + h\dot{\boldsymbol{p}} - \boldsymbol{p}_{obs})^\top$ and $N = \|\boldsymbol{p} + h\dot{\boldsymbol{p}} - \boldsymbol{p}_{obs}\|^2$. By substituting (9) into (8), The constrained optimal control problem is described as

$$\begin{aligned} I_1 = \min_{\mathbf{u}_p} & \frac{1}{2}\boldsymbol{\Phi}^\top \boldsymbol{\Phi} + h^2 \boldsymbol{\Phi}^\top \mathbf{u}_p + \frac{h^4}{8}\mathbf{u}_p^\top \mathbf{u}_p, \\ & \text{subject to} \quad \mathbf{M}^\top \mathbf{u}_p \geq (D^2 - N), \end{aligned} \quad (16)$$

where $\boldsymbol{\Phi} = (\boldsymbol{p} - \boldsymbol{p}_d) + h(\dot{\boldsymbol{p}} - \dot{\boldsymbol{p}}_d)$. The Karush–Kuhn–Tucker (KKT) theorem provides an analytical method for solving this optimization problem. To apply this theorem, the constraints from Eq.(15) must be rewritten in the following form

$$q_{ik} = -u_{p_k} + u_{p_{ik}}^{low} \leq 0 \quad k = 1,2,3, \quad i = 1,..,n. \quad (17)$$

where n represents the number of obstacles and $u_{p_{ik}}^{low}$ is the upper bound of constraint. Therefore, the optimality conditions according to the KKT theorem can be written as follows (Jamshidi and Mirzaei, 2024; Najjari et al., 2022)

$$\frac{\partial I_1}{\partial u_{p_k}} + \sum_{i=1}^{n} \lambda_{ik} \frac{\partial q_{ik}}{\partial u_{p_k}} = 0, \qquad k = 1,2,3 \quad (18a)$$

$$\lambda_{ik} q_{ik} = 0, \qquad i = 1,2 \quad (18b)$$

$$q_{ik} \leq 0, \qquad i = 1,2 \quad (18c)$$

$$\lambda_{ik} \geq 0. \quad (18d)$$

where λ_{ik} denotes the Lagrange multiplier related to the constraints. Using the constraints (17), Eq. (18a) can be expressed as follows:

$$\frac{\partial I_1}{\partial \boldsymbol{u_p}} = \mathbf{c}. \quad (19)$$

For further explanations on the KKT optimization conditions, additional details are provided by Jamshidi et al. (2023). Finally the closed-form expression of the constrained control law, in terms of the vector $\boldsymbol{c}$, is obtained as

$$\boldsymbol{u}_p = -\frac{2}{h^2}[\boldsymbol{p} - \boldsymbol{p}_d + h(\boldsymbol{v} - \dot{\boldsymbol{p}}_d) - \frac{h^2}{2!}\ddot{\boldsymbol{p}}_d] + \frac{4}{h^4}\mathbf{c}. \quad (20)$$

Considering Eq.(7), the rotor-generated thrust is computable from the virtual control input vector from Eq. (20). Thus

$$f_T = m\sqrt{(u_z + g)^2 + u_x^2 + u_y^2}. \quad (21)$$

The control signal f_T will be applied directly to manage the quadrotor's motion. The remaining reference angle trajectories, namely ϕ_d and θ_d, can be derived directly from the translational motion as

$$\begin{aligned} \phi_d &= \arctan\left(\frac{\cos\theta_d\,(u_x \sin\psi_d - u_y \cos\psi_d)}{u_z + g}\right), \\ \theta_d &= \arctan\left(\frac{u_x \cos\psi_d + u_y \sin\psi_d}{u_z + g}\right). \end{aligned} \quad (22)$$

Finally, the reference trajectory for tracking has been finalized and transferred to the rotational subsystem.

3.2 Attitude Loop

The outer-loop control defines the desired state for the inner-loop, which uses a nonlinear predictive controller to track these states while considering torque constraints. Similar to the previous section, the Euler angles have a relative degree of $k = 2$, where the control input first explicitly appears. The Taylor series expansion of the angular attitude vector and the desired one is expressed as (Jamshidi et al., 2024)

$$\boldsymbol{\xi}(t+\rho) = \boldsymbol{\xi}(t) + \rho\dot{\boldsymbol{\xi}}(t) + \frac{\rho^2}{2!}\ddot{\boldsymbol{\xi}}(t), \tag{23a}$$

$$\boldsymbol{\xi}_d(t+\rho) = \boldsymbol{\xi}_d(t) + \rho\dot{\boldsymbol{\xi}}_d(t) + \frac{\rho^2}{2!}\ddot{\boldsymbol{\xi}}_d(t), \tag{23b}$$

where ρ represents the prediction time. By substituting Equations (3b) and (5) into (23a), the following equation is obtained:

$$\begin{aligned}\boldsymbol{\xi}(t+\rho) =& \boldsymbol{\xi} + \rho \boldsymbol{T}_{(\boldsymbol{\phi},\boldsymbol{\theta})}\boldsymbol{\Omega} \\ &+ \frac{\rho^2}{2}\left[\boldsymbol{T}_{(\boldsymbol{\phi},\boldsymbol{\theta})}\left(\boldsymbol{f} + \boldsymbol{J}^{-1}\boldsymbol{\tau}\right) + \dot{\boldsymbol{T}}_{(\boldsymbol{\phi},\boldsymbol{\theta})}\boldsymbol{\Omega}\right].\end{aligned} \tag{24}$$

At this stage, the performance index is defined to penalize the next-step tracking error as follows:

$$I_2(\tau(t)) = \frac{1}{2}\left[\boldsymbol{\xi}(t+\rho) - \boldsymbol{\xi}_d(t+\rho)\right]^\top \left[\boldsymbol{\xi}(t+\rho) - \boldsymbol{\xi}_d(t+\rho)\right]. \tag{25}$$

The quadrotor motors can generate a limited torque. Thus, the following condition holds for the control torque vector:

$$\boldsymbol{\tau}^{\min} \leq \boldsymbol{\tau} \leq \boldsymbol{\tau}^{\max}. \tag{26}$$

In the above equation, $\boldsymbol{\tau}^{\min} \in \mathbb{R}^3$ and $\boldsymbol{\tau}^{\max} \in \mathbb{R}^3$ represent the control input constraints defined based on motor capacity. Now, the constrained control law is determined by minimizing the performance index (25), while ensuring that the constraint (26) is satisfied. By applying KKT theorem, the final form of the constrained control law, using Lagrange multiplier vector $z \in \mathbb{R}^3$, is expressed as

$$\begin{aligned}\tau =& -\frac{2}{\rho^2}\boldsymbol{J}^{-1}\boldsymbol{T}^{-1}_{(\boldsymbol{\phi},\boldsymbol{\theta})}\Big[\boldsymbol{\xi} - \boldsymbol{\xi}_d + \rho(\boldsymbol{T}_{(\boldsymbol{\phi},\boldsymbol{\theta})}\boldsymbol{\Omega}) - \rho\dot{\boldsymbol{\xi}}_d \\ &+ \frac{\rho^2}{2}(\dot{\boldsymbol{T}}_{(\boldsymbol{\phi},\boldsymbol{\theta})}\boldsymbol{\Omega} + \boldsymbol{T}_{(\boldsymbol{\phi},\boldsymbol{\theta})}\boldsymbol{f})\Big] - \frac{\rho^2}{2}\ddot{\boldsymbol{\xi}}_d \\ &+ \frac{4}{\rho^4}\boldsymbol{J}^{-1}\boldsymbol{T}^{-1}_{(\boldsymbol{\phi},\boldsymbol{\theta})}\boldsymbol{T}^\top_{(\boldsymbol{\phi},\boldsymbol{\theta})}\boldsymbol{J}^\top z.\end{aligned} \tag{27}$$

4. STABILITY ANALYSIS

In this section, the stability of both the inner and outer controllers is thoroughly analyzed to ensure their robustness and effectiveness within the control system.

4.1 Outer controller stability

Theorem 1. The UAV dynamics in Eq. (2a) remain uniformly bounded under the control law (20), even with the constraints (26). Additionally, to ensure the response converges to a compact set, the prediction time must not exceed a certain limit.

proof. By applying the control law (20) to the system dynamics (2a), the resulting closed-loop dynamics for the position can be expressed as

$$\ddot{\boldsymbol{e}} + \frac{2}{h}\dot{\boldsymbol{e}} + \frac{2}{h^2}\boldsymbol{e} = \frac{4}{h^4}\mathbf{c}, \tag{28}$$

where $\boldsymbol{e} = \boldsymbol{p} - \boldsymbol{p}_d$ is the tracking error.The right-hand side of Eq. (28) represents a bounded perturbation due to constrained control inputs and nonzero Lagrange multipliers. Given their bounded nature in the convex optimization problem, the attitude dynamics can be reformulated as a second-order differential equation. Solving this equation and applying the comparison lemma yields

$$\boldsymbol{e}_i(t) \leq Be^{-\frac{t}{H}}\left(\sin\frac{t}{h} + \eta\right) + \frac{\delta_i h^2}{2}. \tag{29}$$

Since h is positive, it follows that

$$\lim_{t\to\infty} e_i = \frac{\delta_i h^2}{2}. \tag{30}$$

By selecting h such that $h^2 < \frac{2\delta_i}{\epsilon_i}$, e_i remains within $\|e_i\| < \epsilon_i$, making h a crucial parameter in position convergence. The boundedness of $\dot{e}(t)$ is analyzed using the following Lyapunov function:

$$V = \frac{1}{h^2}\boldsymbol{e}^\top\boldsymbol{e} + \frac{1}{2}\dot{\boldsymbol{e}}^\top\dot{\boldsymbol{e}} > 0. \tag{31}$$

Taking its time derivative, we obtain

$$\dot{V} = -\frac{2}{h}\dot{\boldsymbol{e}}^\top\dot{\boldsymbol{e}} + \frac{4}{h^4}\dot{\boldsymbol{e}}^\top\mathbf{c}. \tag{32}$$

From (32), applying the inequality $ab \leq da^2 + \frac{b^2}{4d}$ with $d = \frac{1}{h}$ results in

$$\dot{V} \leq -\frac{1}{h}\|\dot{\boldsymbol{e}}^\top\|^2 + \frac{4}{h^7}\|\mathbf{c}\|^2. \tag{33}$$

Considering the upper bound

$$\|\mathbf{c}\|^2 < \mu, \tag{34}$$

yields

$$\dot{V} \leq -\frac{1}{h}\|\dot{\boldsymbol{e}}\|^2 + \frac{4}{h^7}\mu^2. \tag{35}$$

Using $\|e_i\| < \epsilon_i$ and Eq.(31), this can be rewritten as

$$\dot{V} \leq \frac{-2}{h}V + L. \tag{36}$$

where $L = \frac{2}{h^3}\|\boldsymbol{\epsilon}\|^2 + \frac{4}{h^7}\mu^2$. Solving (36) and using the comparison lemma gives

$$V \leq (V(0) - \frac{hL}{2})e^{\frac{-2}{h}t} + \frac{hL}{2}. \tag{37}$$

Since $h > 0$, the Lyapunov function remains bounded as

$$\lim_{t\to\infty} V = \frac{hL}{2}. \tag{38}$$

It follows that both V and $\dot{\boldsymbol{e}}$ are bounded. This completes the proof. □

Remark 1. Selecting the Taylor series order equal to the system's relative degree (e.g., $k = 2$) ensures accurate tracking performance, even under fast maneuvers. The truncation error remains negligible, and asymptotic stability is guaranteed in the absence of input constraints (Gharamaleki et al., 2020).

4.2 Inner controller stability

Theorem 2. The quadrotor UAV dynamics, as given in Eq. (2b), remain uniformly bounded when the constrained control law (27) is applied.

Proof. The closed-loop dynamics are obtained by incorporating the controller (27) into the system equation,

$$\ddot{\boldsymbol{\varepsilon}} + \frac{2}{\rho}\dot{\boldsymbol{\varepsilon}} + \frac{2}{\rho^2}\boldsymbol{\varepsilon} = \frac{4}{\rho^4}\boldsymbol{T}^{-\top}_{(\boldsymbol{\phi},\boldsymbol{\theta})}J^\top c + \boldsymbol{T}_{(\boldsymbol{\phi},\boldsymbol{\theta})}\boldsymbol{\tau}_{\mathrm{d}}. \tag{39}$$

where $\boldsymbol{\varepsilon} = \boldsymbol{\xi} - \boldsymbol{\xi}_d$ is the vector of tracking error. By defining $\kappa_i = 1, 2, 3$ for the ith element of the vector $\frac{4}{\rho^4}\boldsymbol{T}^{-\top}_{(\boldsymbol{\phi},\boldsymbol{\theta})}J^\top c + \boldsymbol{T}_{(\boldsymbol{\phi},\boldsymbol{\theta})}\boldsymbol{\tau}_{\mathrm{d}}$ in Eq. (39), the error dynamics can be rewritten as follows:

$$\ddot{\boldsymbol{\varepsilon}}_i + \frac{2}{\rho}\dot{\boldsymbol{\varepsilon}}_i + \frac{2}{\rho^2}\boldsymbol{\varepsilon}_i = \kappa_i. \tag{40}$$

As the expression on the right side of the error dynamics in Eq. (40) remains bounded, the proof follows the same approach as in Theorem 1. □

5. SIMULATION RESULTS AND PERFORMANCE EVALUATION

This section evaluates the proposed controller's reliability in handling obstacle avoidance and torque limits through MATLAB simulations, and compares its performance with SMPC. The discrete-time SMPC method (Kang et al., 2021) has been extended in this study to accommodate quadrotors while explicitly incorporating spatial constraints. The prediction time was set to $h = 0.1$ for the outer controller and $\rho = 1.1$ for the inner controller.

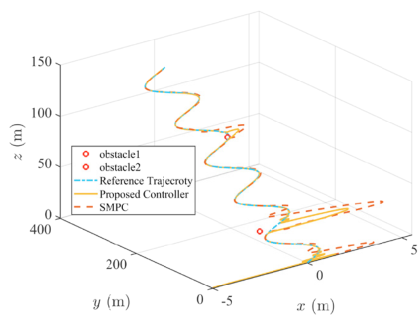

Fig. 2. Comparison results of path tracking in propose method and SMPC.

To introduce real-world uncertainties, the thrust input was perturbed by a time-varying disturbance modeled as

$$\delta(t) = 0.06\sin(2\pi t) + 0.06\sin(\pi t)$$

In addition, external disturbances acting on the UAV are modeled as

$$\tau_d = \begin{bmatrix} 0.002(\sin(t) + \sin(0.5t)) \\ 0.002(\cos(0.5t) - \cos(0.8t)) \\ 0.002(\sin(t)\cos(0.8t)) \end{bmatrix}.$$

Sensor imperfections were introduced through gyroscope noise, including an angle random walk (ARW), bias instability, and a constant bias offset of approximately. Additionally, two no-fly zones are considered at the coordinates $\boldsymbol{p}_{obs_1} = [0.9, 253, 75]^\top$ and $\boldsymbol{p}_{obs_2} = [-1, 75, 23]^\top$. The comparison results of the proposed controller are shown in Figs. 2 to 4. In Fig. 2, the trajectory of the quadrotor is illustrated, demonstrating its capability to navigate the environment while maintaining a safe distance from restricted zones. It is observed that SMPC undergoes more intense chattering near the no-fly zones. In contrast, the proposed controller provides a smoother response while strictly enforcing constraints.

Euler attitudes tracking and control inputs, presented in Fig. 3, confirm that the applied torques are effectively constrained to 0.2 N·m, ensuring compliance with actuation limits. These results validate the proper implementation of control input constraints. To enforce spatial constraints, the minimum allowable distance between the quadrotor and the no-fly zones is set to 5 meters, as shown in Fig. 4. The magnified section of Fig. 4 illustrates that the quadrotor effectively maintains this distance, as all trajectories remain above the predefined threshold.

The proposed controller exhibits reduced control torque demand compared to SMPC, leading to smoother actuator dynamics. This contributes to lower energy consumption,

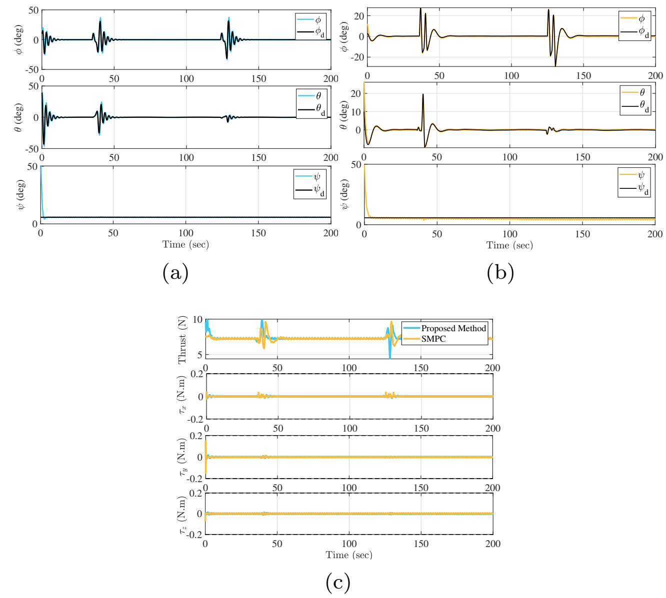

Fig. 3. (a) Euler attitude and desired value (proposed method), (b) Euler attitude and desired value (SMPC), (c) Thrust and control input comparison.

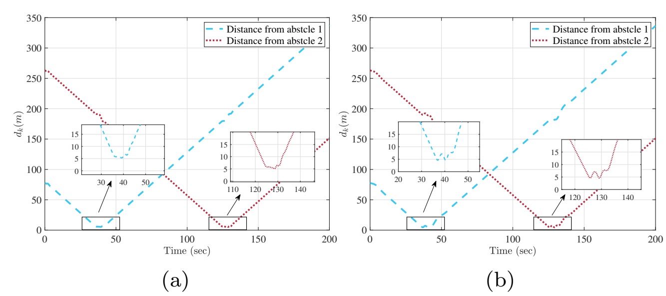

Fig. 4. Distance to no-fly zones: (a) Proposed method, (b) SMPC

mitigated mechanical and thermal stresses, and enhanced longevity of both actuation systems and power electronics. A key advantage of the proposed method is its ability to efficiently forecast future system behavior using Taylor series expansion, without the heavy computational burden of SMPC. This makes it highly suitable for real-time applications.

Another advantage of the proposed approach is the ease of parameter tuning. While SMPC requires intricate parameter adjustments that can be challenging to optimize, the proposed method offers a more intuitive and straightforward tuning process, enhancing its practical applicability in UAV control.

Controller	Proposed Method	SMPC
MSE	2.2281	3.3494
RMSE	1.4927	1.8301
MAE	0.1768	0.3790
Control effort	$[0.4356, 0.4258, 0.4869]^\top$	$[0.4951, 0.4806, 0.5374]^\top$
Comp. Time (s)	1.0829	6.5579

Table 1. Performance evaluation of controllers

The results of the comparison between the two methods are presented in Table 1. The evaluation metrics include mean square error (MSE), root mean square error (RMSE), mean absolute error (MAE), control effort and computation time. According to the data in this table, the proposed method achieves lower error values across all metrics while significantly reducing computation time. These results indicate that the proposed controller not only improves tracking accuracy but also enhances computational efficiency compared to the alternative method.

6. CONCLUSION

This paper presents a continuous constrained predictive control method for quadrotor trajectory tracking, focusing on input limits and obstacle avoidance. The results show that the proposed method tracks the trajectory effectively, handles torque limits, and keeps a safe distance from no-fly zones. It performs better than other methods by reducing energy usage and avoiding unnecessary movements. Additionally, its efficient prediction technique makes it well-suited for real-time applications in dynamic and complex environments.

REFERENCES

Cabecinhas, D., Cunha, R., and Silvestre, C. (2014). A nonlinear quadrotor trajectory tracking controller with disturbance rejection. *Control Engineering Practice*, 26, 1–10.

Gharamaleki, R. M., Mirzaei, M., Rafatnia, S., and Alizadeh, B. (2020). An analytical approach to optimal control of nonlinear systems with input constraints. *International Journal of Automation and Control*, 14(2), 213–238.

Jamshidi, S., and Mirzaei, M. (2024). Novel scheme for uncertainty and disturbance estimation to control of spacecraft system with input constraint. *Proceedings of the Institution of Mechanical Engineers, Part I: Journal of Systems and Control Engineering*, 238(10), 1738–1751.

Jamshidi, S., Mirzaei, M., and Malekzadeh, M. (2023). Applied nonlinear control of spacecraft simulator with constraints on torque and momentum of reaction wheels. *ISA Transactions*, 138, 705–719.

Jamshidi, S., Mirzaei, M., and Malekzadeh, M. (2024). Applied optimal control of spacecraft simulator subject to failures of reaction wheels. *Arabian Journal for Science and Engineering*, 49(2), 1697–1712.

Jamshidi, S., Mirzaei, M., Khodaverdian, M., and Castaldi, P. (2025). Perturbation observer-based constrained fault tolerant control of flexible spacecraft using continuous predictive approach. *Control Engineering Practice*, 156, 106210.

Kang, S., Wu, H., Yang, X., Li, Y., Yao, J., Chen, B., and Lu, H. (2021). Discrete-time predictive sliding mode control for a constrained parallel micropositioning piezostage. *IEEE Transactions on Systems, Man, and Cybernetics: Systems*, 52(5), 3025–3036.

Khodaverdian, M., Najafi, M., Kazemifar, O., and Rahmanian, S. (2025). Fault-tolerant model predictive sliding mode control for trajectory replanning of multi-uav formation flight. *Applied Mathematics and Computation*, 487, 129073.

Labbadi, M. and Cherkaoui, M. (2019). Robust adaptive backstepping fast terminal sliding mode controller for uncertain quadrotor UAV. *Aerospace Science and Technology*, 93, 105306.

Lee, H., and Kim, H. J. (2017). Trajectory tracking control of multirotors from modelling to experiments: A survey. *International Journal of Control, Automation and Systems*, 15(1), 281-292.

Li, B., Ji, Z., Zhao, Z., and Yang, C. (2025). Model predictive optimization and terminal sliding mode motion control for mobile robot with obstacle avoidance. *IEEE Transactions on Industrial Electronics*.

Lin, M., Li, B., Zhou, B., and Cecati, C. (2024). Distributed stochastic model predictive control for heterogeneous UAV swarm. *IEEE Transactions on Industrial Electronics*.

Nadales, J. M., Hakobyan, A., de la Peña, D. M., Limon, D., and Yang, I. (2024). Risk-aware Wasserstein distributionally robust control of vessels in natural waterways. *IEEE Transactions on Control Systems Technology*, 32(4), 1471–1478.

Najjari, B., Mirzaei, M., and Tahouni, A. (2022). Decentralized integration of constrained active steering and torque vectoring systems to energy-efficient stability control of electric vehicles. *Journal of the Franklin Institute*, 359(16), 8713–8741.

Vargas, S., Becerra, H. M., and Hayet, J. B. (2022). MPC-based distributed formation control of multiple quadcopters with obstacle avoidance and connectivity maintenance. *Control Engineering Practice*, 121, 105054.

Wang, B., Zhang, Y., and Zhang, W. (2022). Integrated path planning and trajectory tracking control for quadrotor uavs with obstacle avoidance in the presence of environmental and systematic uncertainties: Theory and experiment. *Aerospace Science and Technology*, 120, 107277.

Wang, D., Pan, Q., Shi, Y., Hu, J., and Zhao, C. (2021). Efficient nonlinear model predictive control for quadrotor trajectory tracking: Algorithms and experiment. *IEEE Transactions on Cybernetics*, 51(10), 5057-5068.

Wang, Y. and Boyle, D. (2024). Constrained reinforcement learning using distributional representation for trustworthy quadrotor UAV tracking control. *IEEE Transactions on Automation Science and Engineering*.

Wang, S., Wang, Y., Miao, Z., Wang, X., and He, W. (2024). Dual model predictive control of multiple quadrotors with formation maintenance and collision avoidance. *IEEE Transactions on Industrial Electronics*.

Wen, N., Zhao, L., Su, X., and Ma, P. (2015). Uav online path planning algorithm in a low altitude dangerous environment. *IEEE/CAA Journal of Automatica Sinica*, 2(2), 173–185.

Zhao, C., Wang, D., Hu, J., and Pan, Q. (2021). Nonlinear model predictive control-based guidance algorithm for quadrotor trajectory tracking with obstacle avoidance. *Journal of Systems Science and Complexity*, 34(4), 1379–1400.

Yu, X., Zhou, X., and Zhang, Y. (2019). Collision-free trajectory generation and tracking for uavs using markov decision process in a cluttered environment. *Journal of Intelligent & Robotic Systems*, 93, 17–32.